traced to inadequate welding of grids to supports, provision of transverse steel, and splicing of adjacent grid panels. These details can be improved by proper research and analysis.

The chloride concentrations found in concrete-filled steel-grid bridge decks are sufficient to initiate corrosion of the steel. However, none of the grid decks tested showed any surface spalling.

The chloride concentrations found in the reinforced-concrete slab decks of the parkway bridges are sufficient to initiate corrosion of the reinforcing steel. The physical condition of the majority of these bridge decks shows that surface spalling is a serious problem.

The chloride concentrations found in the reinforced-concrete slab decks of the bridges on I-79 showed that 27 percent of the decks sampled contained chlorides in amounts sufficient to initiate corrosion of the reinforcing steel. However, since the oldest deck is only 11 years old and all the decks are in generally good condition, these bridge decks are merely undergoing the preliminary phases of steel corrosion, and surface spalls have not had sufficient time to develop.

The single most important conclusion of this study is that concrete-filled steel-grid bridge decks are effective in providing long serviceability in chloride-containing environments. This is accomplished without the help of waterproofing membranes, coatings on steel, cathodic protection, or any other substances designed to prolong bridge deck life. At the same time, the construction of such decks does not require high-caliber quality control.

A review of two bridge biddings in October 1975, indicates that concrete-filled steel-grid decks are economically competitive with reinforced-concrete slab decks. The bid price received for the reinforced-concrete slab decks in the parkway west safety update project [13 350 m^2 (143 560 ft^2) on four bridges] was \$125.60/m^2 (\$11.63/ft^2), including galvanized bars and a waterproofing membrane. The low bid received for the replacement of one 434-m^2 (4669-ft^2) bridge deck was \$139.60/m^2 (\$12.00/ft^2) for a concrete-filled steel-grid deck. Thus, the concrete-filled steel-grid bridge deck may be an economical, lightweight, and durable solution to the problem of bridge-deck deterioration.

ACKNOWLEDGMENTS

We acknowledge the contributions of various engineers who cooperated in providing information and data about existing concrete-filled steel-grid decks. The samples for the chloride test were collected by the bridge inspection staff of District 11-0, and the tests were conducted by the Bureau of Materials and Research, Pennsylvania Department of Transportation. We also acknowledge the cooperation of the Civil Engineering Department of the University of Pittsburgh.

REFERENCES

1. K. C. Clear and R. E. Hay. Time to Corrosion of Reinforcing Steel in Concrete Slabs. Federal Highway Administration, Interim Rept., April 1973, pp. 1-8.
2. D. L. Spellman and R. F. Stratfull. Laboratory Corrosion Test of Steel in Concrete. Division of Highways, California Department of Public Works, Res. Rept. MR-635116-3, Sept. 1968, pp. 1-19.
3. C. F. Stewart. Deterioration in Salted Bridge Decks. In Improving Pavement and Bridge Deck Performance, HRB, Special Rept. 116, Aug. 1971, pp. 23-28.
4. R. F. Stratfull and V. VanMatre. Corrosion Autopsy of a Structurally Unsound Bridge Deck. Division of Highways, California Department of Public Works, Rept. MR-5716-8-72-41, Jan. 1973, pp. 1-17.
5. D. L. Spellman and R. F. Stratfull. Chlorides and Bridge Deck Deterioration. Division of Highways, California Department of Public Works, Interim Rept., Aug. 1969, pp. 1-17.
6. V. Hasija. Concrete-Filled Steel-Grid Floors for Bridges. Reliance Steel Products Co., McKeesport, PA, July 1975, pp. 1-61.
7. C. Angeloff. An Evaluation of the Comparative Effect of Chlorides on the Deterioration of Reinforced-Concrete-Slab and Concrete-Filled-Grid Bridge Decks. Univ. of Pittsburgh, MS thesis, April 1976, pp. 1-62.
8. Standard Specifications for Highway Bridges. AASHO, 1973, Article 1.3.6.
9. H. A. Berman. Determination of Chloride in Hardened Portland Cement Paste, Mortar, and Concrete. Federal Highway Administration, Interim Rept., Sept. 1972, pp. 1-22.

Publication of this paper sponsored by Committee on Corrosion.

Possible Explanation of Concrete Pop-Outs

J. H. Havens and R. C. Deen, Bureau of Highways, Kentucky Department of Transportation

Several years of research relating to damage to concrete and aggregates undergoing freezing and thawing is summarized. Basic principles involving freezing and the attendant pressures are discussed. These principles were applied to the evaluation of concrete in experiments on concretes having low and high air contents. The freeze-thaw characteristics of saturated aggregates relative to their physical properties such as porosity, absorption, and bulk specific gravity were studied by submerging individual particles in prechilled mercury. The pressures associated with pop-outs in concrete were monitored and are discussed in theoretical terms.

Voids occur in concrete through the entrapment and entrainment of air, the occlusion of excess mix water, differences in the specific volumes of reactants and hydration products, leaching of hydration products such as CaO and the use of porous aggregates. Those voids that are easily saturated affect the durability of the concrete unfavorably while those that are less permeable increase the durability. Much water is occluded in concrete in the form of excess mix water and water ab-

sorbed by the aggregate. Concrete that has not been allowed to dry after curing and before the onset of freezing does not perform as well in laboratory tests as does concrete that has been dried, but otherwise is similar. This indicates that a somewhat irreversible fixation or tightening of the mortar structure attends drying so that the concrete becomes less susceptible to resaturation; i.e., the process of drying may close some of the pores. The use of aggregate that is merely moistened, as opposed to soaked or saturated, in the concrete favorably affects its durability—at least in laboratory freeze-thaw tests. Either or both of these effects may be merely the result of delayed saturation.

Dry concrete is unaffected by freezing and thawing: In fact, serious damage is sustained only when a high degree of saturation exists. If the concrete is relatively impermeable, even though it contains a large percentage of voids, saturation is unlikely to occur unless exposure to water is sustained for a long period of time. In natural exposures, periods of wetting alternate with periods of drying, and the durations of the drying periods tend to exceed those of the wetting periods. In the random course of nature, a concrete structure such as a bridge would tend to dry; however, long interim periods of wetness followed immediately by freezing may be extremely damaging.

BASIC THERMAL ANALYSIS

The density of water at 0°C (32°F) is 999.8 kg/m^3 (62.4 lb/ft^3), and the density of ice at 0°C is 917 kg/m^3 (57.2 lb/ft^3) (1). There is an increase in volume of approximately 9 percent when water freezes. If the pores or voids in concrete are completely filled with water and this is frozen, the concrete must dilate or expand proportionally.

Saturation of all voids to 91.7 percent is termed critical saturation, alluding to the degree of saturation beyond which freezing of the water overfills the voids with ice and creates internal expansive pressures. While its theoretical meaning is quite clear, its practical meaning is more in the sense of a statistical average that can be interpreted in two ways: (a) 91.7 percent of the voids are completely filled or (b) all the voids are filled to 91.7 percent of their capacity. The first possibility could be extremely damaging to concrete undergoing freezing; if the second possibility accurately described the condition of the water in the concrete, there would be no damage from freezing.

Analogous Phenomena

To demonstrate some basic principles, preliminary experiments were made on rather idealized models (2). First, water in an open vessel was frozen in air, and a time versus temperature record was made with a thermocouple placed near the center of the volume of water. The resulting thermograph (Figure 1) had a broad step at 0°C with no noticeable depression of the freezing point. Second, a closed vessel or steel bomb was improvised from a 76.2-mm (3-in) diameter pipe nipple and two cast-iron caps. A valve and thermocouple well were tapped into the nipple. The bomb was filled with water and frozen in air as before; the resulting thermograph is also shown in Figure 1. Freezing began at 0°C, the freezing point gradually decreased to -4°C (25°F), and then suddenly the cap ruptured and the temperature increased to 0°C. The pressure at rupture agreed closely with the estimated ultimate strength of the cast-iron caps [48 MPa (7000 lbf/in^2)].

Third, the ruptured cap was replaced, and the bomb was filled with water to 96 percent of its capacity. Here again, the water began to freeze at 0°C, but there was no immediate depression of the freezing point and consequently no immediate increase in pressure. In this case, the development of pressure was delayed until most of the water had frozen. The depression of the final freezing point was 3.3°C (6°F) and the pressure at this point was 43 MPa (6200 lbf/in^2); there was no explosive rupture, but the caps yielded considerably.

Experimental Phenomena

Figure 2 illustrates a typical time versus temperature curve obtained from an oven-dried specimen of concrete undergoing one freeze-thaw cycle. Since the freezing was done in air, the specimen temperature lagged behind the air temperature, and there were no sharp breaks or steps in the cooling curve. On flooding the freezing chamber with water at 4°C (40°F), the temperature of the specimen increased rapidly, but there were no sharp steps or breaks in the curve. Figure 2 also illustrates a typical time versus temperature curve obtained from a highly porous, highly absorptive, highly saturated concrete undergoing one cycle of freeze-thaw. The steps in the freezing and thawing curves occurred at approximately the same temperature—near, but not exactly at, the normal freezing temperature of water. The portions of the curves above and below that step have characteristically different curvatures, and the steps are not merely offsets in otherwise normal cooling and heating curves. The slopes of either or both curves as they approach the step may be described as $\Delta T/\Delta t$, i.e., the incremental change in temperature per increment of time. This factor, when multiplied by the product of the specific heat and the weight of the concrete specimen would give the rate at which heat was being removed from the specimen. The product of the time lapse and the rate of heat removal should correspond approximately to the isothermal change in heat content (ΔH) accompanying freezing of the water in the specimen. From Figure 2, it is also apparent that the freezing step is sloping slightly downward from 0°C, signifying that the water began to freeze at a normal pressure of 98 kPa (1 atm), but finished freezing at -22°C (28°F), which corresponds to the freezing point of pure water at a pressure of approximately 31 MPa (4500 lbf/in^2). Since there is no apparent depression of the initial freezing point, no supercooling or other interference mechanism is evident.

A large part of the water absorbed into concrete at saturation may be regarded as being free water that will freeze and evaporate in much the same way that pure water will; it is this water to which the analysis of freezing-point depression and pressure applies most directly. However, part of the water, in addition to the water of hydration and crystallization, exists in an infinitely more complex state because of internal surface absorption and capillary tensions in the concrete. This part of the water is not expected to have a normal freezing point, and it may be of little or no significance here unless its effects appear as an interference mechanism distorting the prototype thermograph.

The only other serious possibility of an interference mechanism is the effect of dissolved electrolytes on the freezing characteristics of the so-called free water. The most abundant solute in hardened concrete is $Ca(OH)_2$, but its solubility at 0°C is about 1.85 kg/m^3 (0.115 lb/ft^3). If complete saturation and 90 percent dissociation are assumed, this would depress the initial freezing point approximately 0.1°C (0.2°F). Since the solution is saturated, it becomes a eutectic or constant-freezing mixture that should otherwise respond to pressure according to the prototype thermo-

graph. The possible effects of alkali available from the cement may be similarly estimated by assuming 0.6 percent alkali by weight of cement and the maximum free water to be approximately equal to the excess mix water. This quantity of alkali, if available as solute, would depress the initial freezing point a maximum of 1.4°C (2.5°F). Since there are no such initial depressions apparent, the concentration of alkali must be rather small, at least while the greater portion of water is freezing. Alkalies such as NaOH and KOH are much more soluble than $Ca(OH)_2$. In dilute solutions of this type, water freezes into nearly pure ice and concentrates the salts in the remaining solution; this decreases the freezing point of the remaining solution. This type of interference mechanism would cause the freezing point step to curve downward at an increasing rate, and there would be no discrete terminus to the step. A general, but cursory, conception of the effects of pressure and different concentrations of highly soluble electrolytes is compared with the normal freezing curve for pure unrestrained water in Figure 3.

In another experiment, two sets of 152-mm (6-in) cubes were cast using a six-bag mix, a 76-mm (3-in) slump, and a dense limestone aggregate. One set contained 13 percent air; in the other set, the concrete was vibrated to expel the entrapped air and had a final air content of 0.7 percent. The two sets of specimens represent extremes of air contents and were a deliberate attempt to magnify the effects of the air contents on the thermographs. Three thermocouples were cast into these specimens to measure their freezing points. One specimen from each of the two sets was moist cured for 5 weeks before the beginning of freeze-thaw, and these specimens failed to exhibit any indication of a freezing-point step even after 30 cycles. The other specimens of each set were cured 14 d and immersed in water for 24 h before the beginning of freeze-thaw. These specimens showed a progressive broadening of the step and a progressive differentiation between the air-entrained and the non-air-entrained concretes, indicating that the rate of absorption of water by the non-air-entrained concrete was much greater. Freeze-thaw was continued to 77 cycles, at which time the non-air-entrained specimens were virtually ruined. Thermographs of the first, fortieth, and seventy-seventh cycles are shown in Figure 4.

The failure of the two concrete specimens that were cured 5 weeks to exhibit a significant thermal step, even after 30 cycles of freeze-thaw, offers an example of highly retarded or delayed saturation. Continued curing and hydration tend to desiccate the smaller interstices of the cement gel and reduce the free water content of the concrete. Continued curing would likewise densify and strengthen the mortar against subsequent ingresses of water. Thus, the mere number of freeze-thaw cycles that a concrete specimen is able to withstand before saturation becomes critical is probably not as significant as the time duration of the conditions causing absorption of water and eventual saturation. It is suggested, therefore, that the number of regular cycles or the time preceding the development of a significant thermal step and freezing-point depression may be a significant basis for evaluating concrete durability.

Figure 1. Typical thermographs.

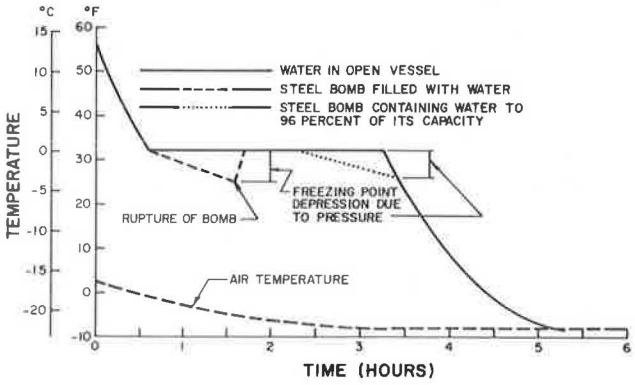

Figure 2. Typical time versus temperature curves of concrete undergoing single freeze-thaw cycle.

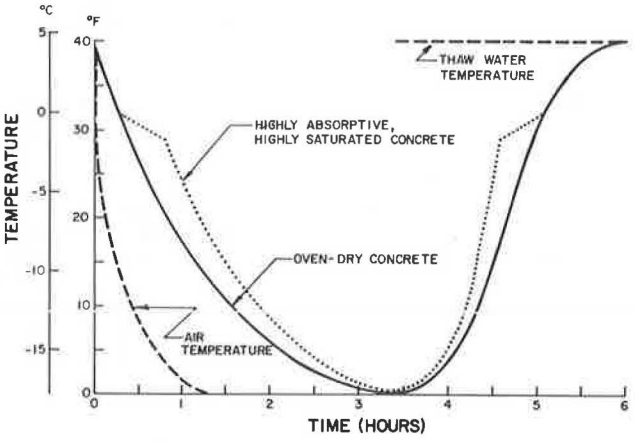

Figure 3. Probable effects of solutes on time versus temperature curve.

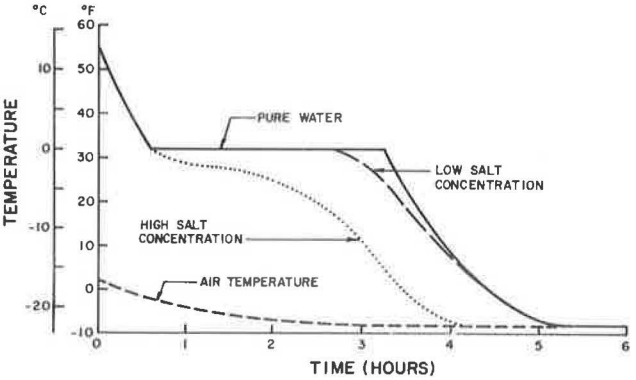

FREEZE-THAW RESISTANCE OF AGGREGATES

The present methods for testing aggregates use composite samples, and the results of such tests provide average values. For example, the average value of absorption obtained from a composite sample may have a low value indicating a sound aggregate; however, if each particle were analyzed, it might be found that a portion of the aggregate was so highly absorptive as to be detrimental to concrete. The percentage of these deleterious particles in an aggregate is also important. Logically, in determining the soundness of an aggregate sample, the freeze-thaw testing should be conducted on a per-particle basis. Each particle should be saturated at the onset of testing and kept saturated during testing. For study purposes, the degree of saturation may be varied. Maximum saturation definitely establishes the ultimate susceptibility of the aggregate to damage from freezing and thawing.

Figure 4. Time versus temperature curves of concrete containing 0.7 and 13 percent air moist-cured 14 d and soaked 24 h.

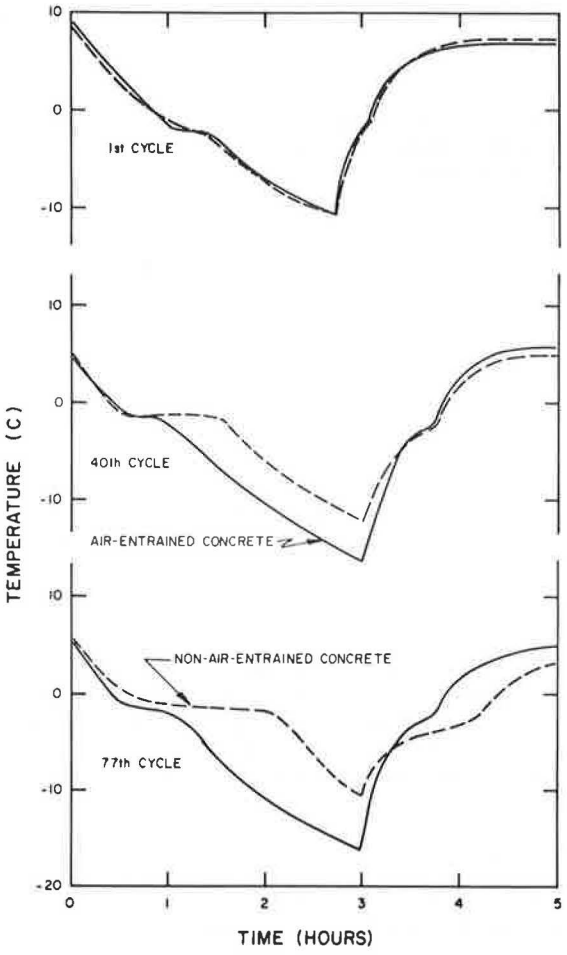

Figure 5. Cumulative percentage of fractured particles.

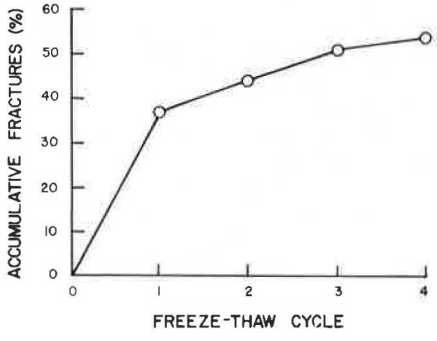

Figure 6. Relation between particle size and percentage of fractured particles after exposure to four freeze-thaw cycles.

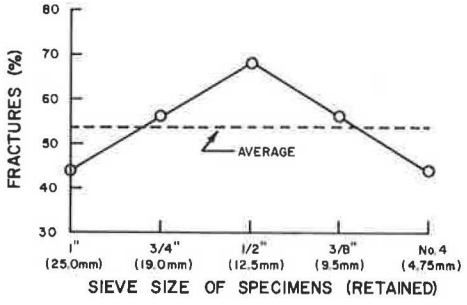

Phenomena

To obtain objective data—definitive relations between the effects of freezing and thawing and such physical properties as porosity, absorption, and bulk specific gravity—pertaining to the freeze-thaw characteristics of aggregate, the following conditions were required (3): (a) a freezing medium in which each aggregate particle could be frozen quickly so that the quickly frozen surface would form a seal or shell about the particle and retain the pore water and (b) a medium that would not contaminate the pore water. Chilled mercury was chosen as the freezing medium—it has a high thermal conductivity, it is immiscible with water, and it has a low freezing point. The test consisted of submerging the aggregate particle in prechilled mercury. Preliminary testing showed that if a particle did not show visual distress at the end of four cycles—which could be performed in a matter of minutes—it would withstand innumerable cycles.

A saturated gravel that represented a variety of rock types and possessed a wide range of physical properties was secured from a glacial outwash deposit and kept inundated to ensure saturated conditions. The primary constituents of the aggregate sample were dolomites, cherts, limestones, sandstones, siltstones, and various igneous and metamorphic rock particles. Although usually acceptable for concrete, this gravel contained both sound and unsound particles and provided an appropriate assortment of particles.

After grading according to five sizes ranging from 4.75 to 38.1 mm (no. 4 sieve to 1.5 in), each particle was numbered. For each particle, the saturated-surface dry weight and the bulk volume, by mercury displacement, were measured before the freeze-thaw tests, and the bulk specific gravity was calculated. The freezing was accomplished by submerging each particle in cold mercury [-30 to -35°C (-22 to -31°F)] for 5 min. The mercury was contained in a glass cylinder enclosed in an insulated container of dry ice (solid CO_2). At the end of each freezing cycle, the particle was removed from the mercury, placed in a container of water, and allowed to thaw. At the end of each thawing cycle, the particle was examined visually and any distress resulting from the freezing and thawing was recorded.

Absorption values for each particle were determined after the freeze-thaw testing. Each particle (or major piece) was dried to a constant weight at 110°C (230°F). The absorption of each particle was calculated from

$$w = 100(W_T - W_S)/W_S \quad (1)$$

where

w = absorption (percent),
W_T = saturated-surface dry weight of particle (or major pieces), and
W_S = oven-dried weight of particle (or major pieces).

Porosity calculations were made by using

$$\eta = 100G_{SSD}\, w/(100 + w) \quad (2)$$

where η = porosity (percent) and G_{SSD} = bulk specific gravity (saturated-surface dry). (This equation applies only for saturated aggregates.)

The accumulated number of fractured particles at the end of each freeze-thaw cycle, expressed as a percentage of the total number of particles, is shown in Figure 5. Of the total number of fractures, approximately 70 percent occurred during the first freezing cycle. The small increases in the accumulated percentage of frac-

tured particles that occurred after succeeding cycles are probably due to fractures that were undetected at the end of the first freezing cycle and required additional cycles before they became visible.

The percentage of fractured particles at the end of the fourth cycle of freeze-thaw, for each particle size tested, is shown in Figure 6. The largest percentage of fractured particles occurred in the 12.5-mm (0.5 in) size; the smallest percentages occurred in the 25 and 4.75-mm (1-in and no. 4) sizes. The average percentage of fractured particles of all sizes combined was 53.6. The 25-mm particles were mostly igneous and metamorphic rock particles that, by their mode of formation, are less porous than water-lain sedimentary rocks. Most of the 12.5-mm particles were porous cherts and dolomites. Most of the 4.75-mm particles were quartz.

The relation between the soundness of the test particles and their adjusted porosity values is shown in Figure 7. As expected, the more porous particles were less durable than the less porous particles. All particles having a porosity of more than 11 percent fractured in the freeze-thaw test; less than 25 percent of the particles having a porosity of less than 2 percent fractured.

The relation between the percentage of fractured particles and the absorption values of the test particles is also shown in Figure 7. All particles having absorptions of 4 or more percent failed when subjected to freezing and thawing. Very few specimens having absorptions of less than 1 percent failed. Between these extremes, the percentage of particles failing increased as the absorption increased.

Theory

The ability of a rock fragment to withstand the internal pressures that accompany freezing is controlled by certain inherent properties of the fragment. These properties can be understood in terms of Timoshenko's explanation (4) of Lame's solution for the radial and tangential stresses in a thick-walled, spherical container under internal and external pressures. If the exterior confining pressure (P_o) is zero, Timoshenko's equation for radial stresses (σ_r) at the extreme outer fiber is

$$\sigma_r = 0 \tag{3}$$

Figure 7. Relation between porosity and absorption and percentage of fractured particles after exposure to four freeze-thaw cycles.

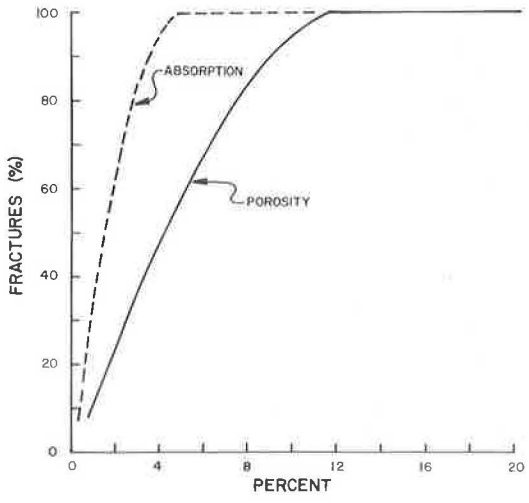

For tangential stresses (σ_t), Timoshenko's equation reduces to

$$\sigma_t = 3P_i a^3/2(a^3 - b^3) \tag{4}$$

where

P_i = internal pressure,
a = inner radius of sphere, and
b = outer radius of sphere.

If

$$V_v = 4\pi a^3/3 = \eta V_t \tag{5}$$

and

$$V_t = 4\pi b^3/3 \tag{6}$$

where

V_v = volume of voids,
V_t = total volume of sphere, and
η = porosity = V_v/V_t are substituted in Equation 4, it becomes

$$\sigma_t = 3P_i\eta/2(1 - \eta) \tag{7}$$

σ_r along the outer edge of the spherical container is zero, and σ_t at the same point, which is a tensile stress, is dependent on the porosity and tensile strength of the container and independent of its size or total volume.

If σ_t is replaced by the tensile strength (σ_u), Equation 7 becomes

$$P_u = 2\sigma_u(1 - \sigma)/3\sigma \tag{8}$$

where P_u = maximum allowable internal pressure. The tensile strengths of the gravel particles were not determined, but similar materials have tensile strengths ranging from 0.7 to 7 MPa (100 to 1000 lbf/in^2). If the tensile strength is known, the maximum allowable internal pressure for various porosity values can be calculated. Porosity-pressure curves for tensile strengths of 2, 4, and 6 MPa (300, 600, and 900 lbf/in^2) are shown in Figure 8.

The determination of the internal pressure accompanying the freezing of water within a hollow sphere can also be approached from a theoretical standpoint. If the temperature-volume changes of the sphere, water, and ice are neglected, the volume of ice (V_I) within the cavity, assuming all the water freezes, is

$$V_I = 4\pi a^3 S(1 + \beta)(1 - P_i K)/3 \tag{9}$$

where

S = degree of saturation,
β = volume increase accompanying freezing of water, and
K = bulk modulus of ice.

The tangential strain at any point within the sphere is given by

$$\epsilon_t = \delta/r = (\sigma_t/E) - \mu(\sigma_r/E) \tag{10}$$

where

ϵ_t = tangential strain,
δ = radial displacement,

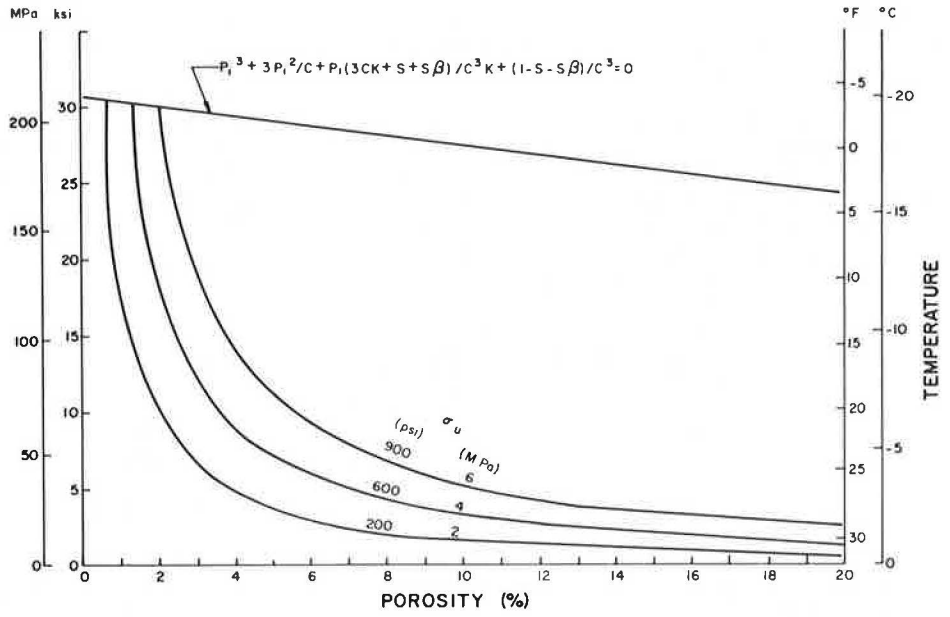

Figure 8. Suggested theoretical relations for varying tensile strengths.

E = Young's modulus of elasticity of sphere,
μ = Poisson's ratio of sphere, and
r = radial distance.

By assuming that $P_o = 0$ and substituting for V_v and V_t, the increase in the radius of the internal cavity or void due to an internal pressure reduces to

$$\delta = aP_i(1 + \mu + 2\mu - 4\mu\eta)/2E(1 - \eta) \quad (11)$$

The volume of the cavity (V_c) under internal pressure will thus increase to

$$V_c = 4\pi a^3(C^3P_i^3 + 3C^2P_i^2 + 3CP_i + 1)/3 \quad (12)$$

where $C = (1 + \mu + 2\mu - 4\mu\eta)/2E(1 - \eta)$. The volume of the ice within the cavity must be equal to the volume of the cavity. By equating the two and rearranging, it follows that

$$P_i^3 + (3P_i^2/C) + [P_i(3CK + S + S\beta)/C^3K] + (1 - S - S\beta)/C^3 = 0 \quad (13)$$

The internal pressure was calculated for various porosity values by using the following values: $\mu = 0.365$, E = 6.9 GPa (1 000 000 lbf/in^2), K = 8.3 GPa (1 200 000 lbf/in^2), S = 1.00, and $\beta = 0.0917$. This plot is superimposed on the maximum allowable internal pressure curves in Figure 8.

The intercepts of the maximum and the available pressure curves are the maximum safe-porosity values. At porosities greater than these, rupture will occur at less than the maximum available pressure. Pressure is dependent on temperature, and as the porosity increases, less pressure—and consequently less severe temperatures—will cause failure. Figure 8 also shows the theoretical relations among disruptive temperature, porosity, and tensile strength. For a given tensile strength, the disruptive temperature increases as the porosity increases, and rupture may occur at a temperature slightly below freezing if the porosity is high.

The range over which critical porosity occurs is a manifestation of the inherent tensile strength of the aggregate. Whereas it must be presumed that tensile strength varies in inverse proportion to porosity, the inherent tensile strength varies within a wide range that depends on the mineralogical nature of the aggregate. Hence, the force opposing the expansion accompanying freezing—and therefore the limiting pressure—is governed by the restraining strength of the aggregate or the confining vessel. Logically, an encasement medium such as mortar or concrete will provide additional restraint against the forces emanating from a dilating particle of aggregate. Thus, restraint increases with depth of embedment. A saturated particle of aggregate in concrete may be viewed as being a center of compression, and the surrounding concrete may be viewed as a thick-walled shell or vessel. Of course, at near-surface locations, the restraint is unbalanced, and pop-outs or cracking will result if the dilating pressures are critical.

PRESSURES ASSOCIATED WITH POP-OUTS

Pop-outs and deep-seated deterioration are generally associated with high absorptivity and high saturation. Aggregate particles of all sizes are capable of inducing damaging pressures. Particles that are near the surface may produce pop-outs even though the dilating pressures are relatively low because the surrounding shell of concrete offers only minor restraint.

Phenomena

To gain a better understanding of the mechanisms associated with these signs of distress, failures were induced by subjecting voids of varying diameters and depths below the concrete surface to hydrostatic pressure (5). Concrete specimens [254 by 254 by 102 mm (10 by 10 by 4 in)] were cast from six-bag concrete containing limestone coarse and fine aggregates. The specimens were moist cured at 25°C (77°F) 28 d. Each specimen was then drilled with a flat-faced masonary bit to form a cylindrical hole in the center of one of the 254 by 254-mm surfaces. The hole depths ranged from 63.5 to 93.4 mm (2.5 to 3.875 in) and provided depths of burial ranging from 28.1 to 3.2 mm (1.5 to 0.125 in). The diameters of the bits used for drilling were 6.4, 9.5, 12.7, 19.1, 25.4, and 34.9 mm (0.25, 0.375, 0.5, 0.75, 1, and 1.375 in). A 6.4-mm (0.25-in) high-pressure tube and rubber gasket assembly was placed in each specimen to within 19.1 mm (0.75 in) of the bottom of the void. The tubing and

gasket were held in place with high-strength epoxy cement. In all cases, the void depth was 19.1 mm, and only the void diameter and the depth of burial were varied.

A hand-operated pump capable of producing a maximum pressure of 34 MPa (5000 lbf/in^2) was connected to the pressure tubing, and glycerin was pumped into the artificial void at such a rate that the pressure zone was limited essentially to the pressure cavity. [This method has also been used by Bache and Isen (6) to illustrate failure patterns.] The time required to attain the final pressure was approximately 10 s. The characteristics of a resultant pop-out are illustrated in Figure 9. The pressures required to produce pop-outs in the various specimens are shown by the series of curves in Figure 10, which present data obtained from tests on 150 specimens. Results obtained had a remarkably high degree of duplication. For similar depths of burial, greater pressures were required to produce pop-outs in the smaller diameter cavities than were required for the larger cavities. Figure 10 indicates that a cover of about 23 mm (0.9 in) would be necessary for protection against failure from the pressures expected within a 6.4-mm (0.25-in) cavity, and a cover of approximately 31.8 mm (1.25 in) would be needed for 34.9-mm (1.375-in) cavities. All the pop-outs were predominantly conical, and thinning was more pronounced along the outer surface perimeter of the larger pop-outs. Failure widths for the 19.1 and 25.4-mm (0.75 and 1-in) cavities at varying depths of burial are shown in Figure 11. Failure angles were computed from the fitted curves and are shown in Figure 12. The failure angle is significantly related to the cavity diameter and the depth of burial.

Figure 9. Test specimen showing pop-out.

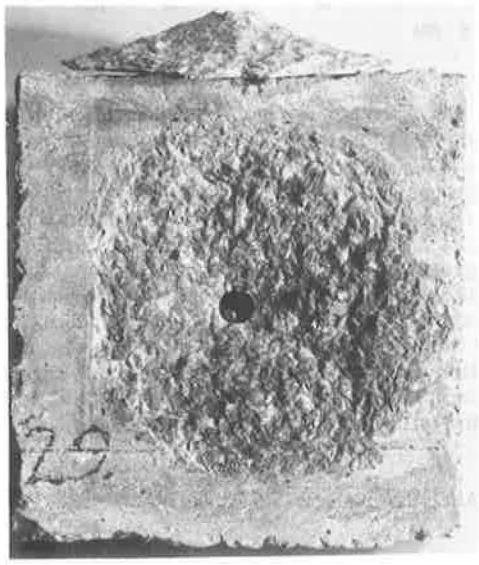

Specimens containing cavities that were more deeply buried split into two sections as shown in the sketch inserted in Figure 13. The pressures required to produce this type failure varied with the cavity diameter but were independent of the depth of burial—that is, above the limit of pop-out failure. The pressures to induce failures of this type did not vary appreciably with the depth of burial because the area of resistance to failure was constant [102 by 254 mm (4 by 10 in)] for all specimens. The limiting depth of burial for a given cavity diameter at which the mode of failure changes is governed by the specimen dimensions, and pop-outs would occur at greater depths of burial in specimens larger than those tested here. Splitting-type failures are represented on the curves in Figure 10 in the zones of zero slope. Failures of this type can be considered as the deep-seated deterioration commonly associated with deeply embedded and highly absorptive aggregate particles. High dilating pressures are necessary for these failures because the restraint on the particles is greater.

Additional tests were conducted by casting water-filled spherical capsules in concrete specimens of the same size as described above. A copper-constantan thermocouple was placed in the center of each sphere of water, and the voltages were amplified and recorded, making possible temperature measurements within $\frac{1}{4}$°C (0.14°F). The pressures accompanying the confined freezing of water within the spheres were computed from

Figure 10. Relations among pop-out pressure, void diameter, and depth of burial.

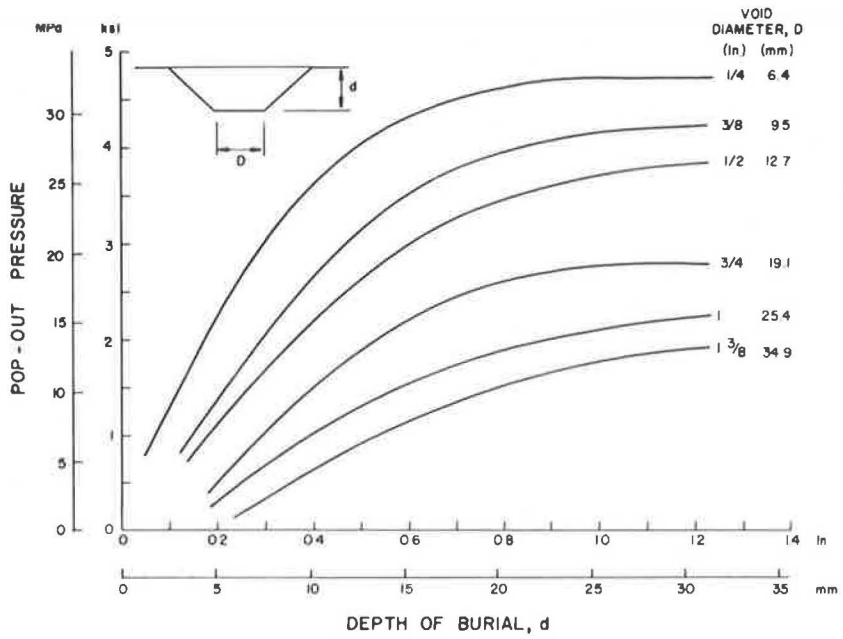

Figure 11. Relations among depth of burial, void diameter, and pop-out width.

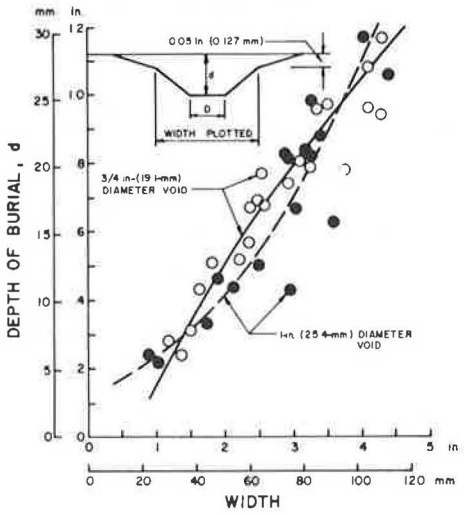

Figure 12. Relation between failure angle and depth of burial.

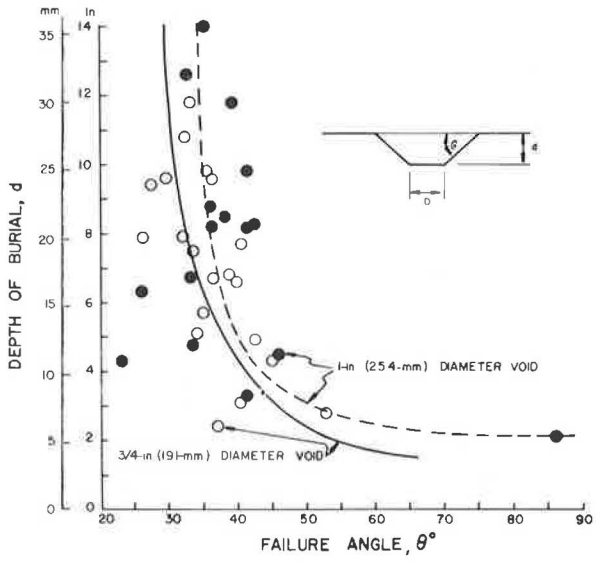

the temperature data. The temperature at failure was -4.0°C (24°F), and the accompanying pressure was 50 MPa (7200 lbf/in^2). After rupture, the pressure decreased, and the freezing point returned to normal. Freezing thereafter was isothermal. These events occurred over a series of successive cycles rather than within a single one. This was interpreted as a manifestation of progressive damage.

Theory

Within a semi-infinite mass, there is a free-field stress distribution. When the continuity of an assumed homogeneous material such as concrete is interrupted by the presence of a porous and saturated aggregate particle undergoing freezing, stresses near the particle are no longer equal to the free-field stresses because there is a discontinuity of strains or deformations at the aggregate-matrix interface. Because of this discontinuity, the induced differential pressures alter the at-rest stress conditions that existed before freezing.

Figure 13. Pressure necessary to produce splitting failure in deeply buried voids.

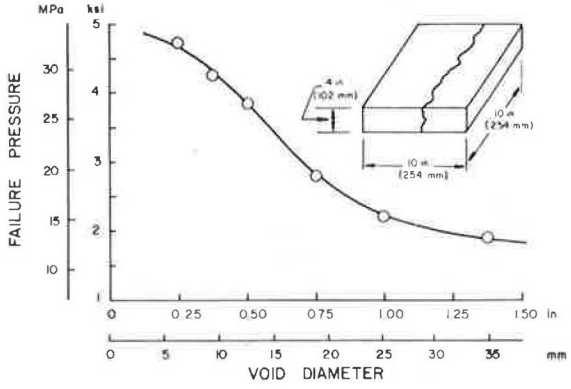

Figure 14. Passive pressures and pop-outs.

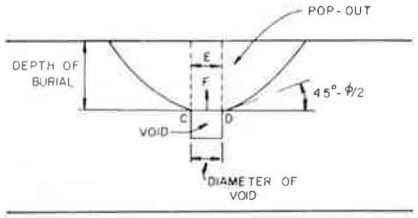

Shear stresses are therefore mobilized within the concrete matrix and, if the shearing strength of the concrete is exceeded, the material may fail in the form of a pop-out.

When a freezing aggregate particle is contained in a concrete mass, relative displacements between the particle and the surrounding matrix will occur, and shearing stresses will be mobilized along those planes that experience shearing distortions. Because of the extremely high pressures that sometimes are developed in freezing aggregate particles, the modulus of the porous particle may be assumed to be greater than that of the surrounding concrete matrix. The resulting conditions may be, in a general way, assumed to be analogous to the phenomenon of stress transference called passive arching.

The application of theoretical solutions implies that the material behaves elastically, but such behavior may depart from ideal at high pressures. However, elastic solutions are good approximations when small displacements are involved. At large displacements, the stresses in some regions will reach the yield stress, and the stress distribution that finally results may be quite different from the stress distribution determined by considering only elastic equilibrium. In Figure 14, the movements of the concrete matrix above plane CD are denoted by arrows E and F. The material just above CD tends to move upward because of the high pressures induced by the freezing and expanding water within the aggregate. The material to the sides of the aggregate particle tends to move laterally, creating a condition analogous to the passive pressure state, i.e., the lateral stresses that occur at the limiting stage of lateral compression. If the deformations proceed far enough and the depth of burial is sufficiently small, the failure surface may propagate to the surface of the concrete mass and result in a pop-out. Rankine's theory gives the passive pressure as

$$P_p = \gamma d \tan^2(45° + \phi/2) + 2c\tan(45° + \phi/2) \qquad (14)$$

where

P_p = passive pressure,
γ = unit mass,
d = depth of burial,
c = cohesion, and
ϕ = angle of friction.

If typical values of 2.4 Mg/m^3 (150 lb/ft^3) for the unit mass of concrete, 7.8 MPa (950 lbf/in^2) for the cohesion, and 47° for the friction angle are used, the passive pressures calculated by Equation 14 are about 33 MPa (4800 lbf/in^2). Because the depth of burial is small, the effect of d in Equation 14 is extremely insignificant. The passive pressures determined from Equation 14 are about the same order of magnitude as the compressive strength of the concrete.

By assuming that passive pressures act over a rectangular surface with dimensions equal to the depth of burial and the void diameter (perpendicular to the plane of the figure), the passive forces can be calculated from Figure 14. If the coefficient of passive pressure is assumed to be 3, the forces acting at the top interface between the void and the concrete mass can be determined, and from this vertical force and the diameter of the void, a calculated value of the void pressure can be obtained. The table below summarizes such calculations for the ranges of depth of burial and void diameter investigated (1 mm = 0.039 in and 1 MPa = 145 lbf/in^2).

Depth of Burial (mm)	Void Diameter (mm)	Void Pressure (MPa)	
		Calculated	Observed
25	25	14.1	14.8
13	25	7.0	9.0
25	35	10.1	8.7
13	35	5.0	6.6
25	6	54.1	32.4
13	6	27.1	27.9

The agreement between the calculated void pressures and the void pressures observed to cause pop-out failure is extremely satisfactory in all except one case, the 25.4-mm (1-in) depth of burial for a void diameter of 6.4 mm (0.25 in).

On the basis of the calculations given above, it seems reasonable to consider the passive-pressure concept as adequate to explain the mode of failure for pop-outs. However, the case of the 6.4-mm diameter void buried 25.4 mm beneath the surface may be different; thus, pressures originating at depths of three or four or more times the cavity size cannot significantly exceed the compressive strength of the concrete.

SUMMARY AND CONCLUSIONS

Aggregates having an absorption greater than 4 percent are likely to rupture on freezing; aggregates having an absorption less than 1 percent are generally unaffected by freeze-thaw. A composite sample of aggregate particles may collectively absorb less than 4 percent water by mass and still contain individual particles having absorptions significantly greater. Absorption tests based solely on composite samples are not adequate in this respect. The degradation of composite samples subjected to saturation and quick freezing cycles could provide a measure of the proportions of sound and unsound particles. Alternatively, each particle within a composite sample could be tested for absorption and the proportions of deleterious material determined statistically.

Concretes can contain as much as 20 percent voids. Theoretically, the critical volume of water in a void is 91.7 percent of saturation (capacity). It is intuitively apparent that the system of voids in a mass of concrete is infinitely complex. It would be possible, therefore, for certain cavities or pores to be critically saturated while others were relatively unsaturated. Here again, gross absorption alone fails to define the state of saturation (unless saturation is complete in all respects). Forced saturation renders concretes and aggregates susceptible to damage through freezing. The entrainment of air causes concrete to be infinitely more difficult to saturate—probably by disconnection of the voids or by the back pressure of air in minute spherical voids. Aggregate particles are usually not immunized in this way and tend to saturate preferentially. Nevertheless, it seems reasonable to conclude that any mechanism by which saturation is delayed or rendered improbable increases the durability of concrete exposed to freezing weather.

REFERENCES

1. N. E. Dorsey. Properties of Ordinary Water-Substance. Reinhold, New York, 1940.
2. J. H. Havens. Thermal Analysis of the Freeze-Thaw Mechanism in Concrete. Engineering Experiment Station, Univ. of Kentucky, Bulletin 59, 1961.
3. J. W. Scott and G. R. Laughlin. A Study of the Effects of Quick Freezing on Saturated Fragments of Rocks. Division of Research, Kentucky Department of Highways, Feb. 1964.
4. S. Timoshenko. Theory of Elasticity. McGraw-Hill, New York, 1934.
5. J. W. Scott, G. R. Laughlin, and J. H. Havens. Freeze-and-Thaw Characteristics of Aggregates. Proc., 16th Annual Highway Geology Symposium, Engineering Experiment Station, Univ. of Kentucky, Bulletin 76, Sept. 1964.
6. H. H. Bache and J. C. Isen. Modal Determination of Concrete Resistance to Pop-Out Formations. Journal, ACI, June 1968.

Publication of this paper sponsored by Committee on Performance of Concrete—Physical Aspects.